JAAS

PAPER

View Article Online
View Journal | View Issue

Cite this: J. Anal. At. Spectrom., 2024, 39, 1094

Natural linewidths of Cu $K\alpha_{1,2}$ spectra obtained with an antiparallel double-crystal X-ray spectrometer

Yoshiaki Ito,†[a] Tatsunori Tochio,[b] Michiru Yamashita,[c] Sei Fukushima,[d] Łukasz Syrocki,[e] Katarzyna Słabkowska,[f] Marek Polasik,[f] José Pires Marques[gh] and Fernando Parente*[i]

To investigate the natural linewidths of Cu $K\alpha_{1,2}$ diagram lines, the spectra of these lines were recorded in detail using an anti-parallel double-crystal X-ray spectrometer. The values obtained for the measured Cu $K\alpha_1$ and $K\alpha_2$ natural linewidths are 2.264(18) eV and 2.534(73) eV, respectively. The contribution of the Coster–Kronig (CK) transition for the $K\alpha_2$ linewidth is found to be approximately 0.27 eV. Theoretical values 2.1454 eV for the $K\alpha_1$ line and 2.1292 eV for the $K\alpha_2$ line were calculated, using the GRASP and FAC codes. A detailed study of the same spectra using Si and Ge crystals and several Bragg surfaces was performed. In addition, the spectral measurements of Cu $K\alpha_{3,4}$ satellite lines were made, and information on the energy values, FWHMs, and intensity ratios of these satellite lines was obtained from multiple-peak fitting analyses.

Received 25th October 2023
Accepted 23rd February 2024

DOI: 10.1039/d3ja00367a

rsc.li/jaas

1 Introduction

Precision measurements of the energies, FWHM, and spectral structures of X-ray line complexes are needed for many purposes in materials sciences. Simultaneous multielectronic transitions within an atom play an important role in determining the structure and the intensities of X-ray emission spectra. This is particularly serious in the case of 3d transition metals, whose asymmetric line shapes were attributed as early as 1928 to contributions from two-electron transitions.[1] Several other mechanisms such as conduction-band collective excitations,[2] exchange,[3] and final-state interactions[4] were also suggested as equally probable alternatives. Despite extensive research efforts over several decades,[5] no final agreement emerged on the physics underlying these line shapes. Recently, combining precise line-shape measurements and *ab initio* relativistic Dirac–Fock calculations, Deutsch's group was able to show that the line shapes of the Cu Kα and Kβ emission lines can be fully accounted for by contributions from 3d spectator–hole transitions only, in addition to the diagram ones.[5] This conclusion was strongly supported by the considerably improved agreement with the theory of L- and M-level widths and fluorescence yields.[6] High-resolution measurements of these spectra photo-excited at energies near the K edge show clearly the first appearance of the asymmetric features at an excitation energy coinciding with the calculated threshold for creation of a [1s3d] two-hole configuration, the initial state of the 3d spectator-hole transitions.[7] These results very convincingly support that the asymmetry of the Cu Kα lines originates from two-electron excitation, but it is clear that, for this interpretation to be conclusive, neighboring 3d elements must be shown to behave similarly.

Ito *et al.*[8,9] measured the $K\alpha_{1,2}$ lines for elements in the range $20 \leq Z \leq 42$, including Cu, using a high-resolution double crystal X-ray spectrometer and, taking into account the instrumental function through Tochio's method,[10] examined the asymmetry and the contribution of [1s3d] shake processes, confirming that, for 3d transition elements, the asymmetry of the $K\alpha_{1,2}$ lines was mainly due to those processes, and evaluated the natural linewidths for each element. In this paper, we extend the measurements reported in ref. 8 to include the element Cu. More recently, Mendenhall *et al.*[11] evaluated the natural width of $K\alpha_{1,2}$ lines and the structure of $K\alpha_{3,4}$ satellite lines using a two channel-cut crystal (+,−; −,+) spectrometer.

[a]*Laboratory of Atomic and Molecular Physics, ICR, Kyoto University, Gokasho, Uji, Kyoto 611-0011, Japan*
[b]*1-24-14 Inadera, Amagasaki 661-098, Hyogo, Japan*
[c]*HIT, 3-1-12 Yukihira, Suma-ku, Kobe 654-0037, Japan*
[d]*Kobe Material Testing Laboratory Co., Ltd, 47-13 Nijima, Harima-cho, Kako-gun, Hyogo 675-0155, Japan*
[e]*Institute of Plasma Physics and Laser Microfusion, Hery 23, 01-497 Warsaw, Poland*
[f]*Faculty of Chemistry, Nicolaus Copernicus University in Toruń, Gagarina 7, 87-100 Toruń, Poland*
[g]*Laboratório de Instrumentação e Física Experimental de Partículas, Av. Prof. Gama Pinto 2, 1649-003 Lisboa, Portugal*
[h]*Faculdade de Ciências da Universidade de Lisboa, Campo Grande, C8, 1749-016 Lisboa, Portugal*
[i]*Departamento de Física, Laboratório de Instrumentação, Engenharia Biomédica e Física da Radiação (LIBPhys-UNL), Faculdade de Ciências e Tecnologia da Universidade Nova de Lisboa, Monte da Caparica, 2892-516 Caparica, Portugal. E-mail: facp@fct.unl.pt*
† Present address: Rigaku Corporation, 14-8, Akaoji-cho, Takatsuki, Osaka 569-1146, Japan.

The presence of hidden satellites, resulting from the shake processes, within the diagram lines, makes it difficult to accurately measure the natural widths, as the measured width depends on the crystal plane used for the measurement. To obtain the natural widths more reliably, we measured the $K\alpha_{1,2}$ lines using several crystal planes with the same crystal spectrometer. To the best of our knowledge, there is no other crystal monochromator capable of making high-resolution spectral measurements suitable for such studies than the two-crystal monochromator.

The Cu $K\alpha_{1,2}$ lines are suitable for analysis, from the angular point of view, through various changes in the crystal plane. Furthermore, as noted by Deutsch *et al.*,[6] the width values of these lines have varied considerably among researchers. The Rietveld method of powder analysis software uses the widths and intensity ratios of these lines. So, these are very important values. Therefore, we measured the Cu $K\alpha_{1,2}$ lines using the Si and Ge planes, (220), (333), and (440), with this high-resolution double crystal X-ray spectrometer and evaluated their natural widths, after taking into account the instrumental function.

Moreover, to investigate the complex structure of the Cu $K\alpha_{1,2,3,4}$ lines in detail, the $K\alpha_{3,4}$ satellite lines were measured using the same spectrometer. Finally, the application to materials based on this multiple-peak analysis will be mentioned.

2 Experimental methodology

The fluorescence $K\alpha_{1,2}$ X-ray spectra of atomic Cu were recorded, by the photon-excitation method, using a RIGAKU double-crystal spectrometer (System 3580E), using various Bragg planes. The instrumental function is explained in detail in ref. 8–10, 12 and 13. An end-window type was adopted with a primary X-ray source of tungsten or rhodium, and the tube operated at 40 kV and 60 mA. Experimental conditions are listed in Table 1. As targets, we used Cu metal plates. The $K\alpha_{1,2}$ spectra were recorded using an $Ar_{0.9}(CH_4)_{0.1}$ gas flow (FPC) and a sealed Xe gas (SPC) proportional counter as a detector. The monochromator used in this work can be considered one of the most stable high-resolution X-ray crystal monochromators that can accurately determine X-ray spectral profiles. The spectrometer can scan a wide 2θ angle range of 20° to 147° without a distortion of the spectral profile. The temperature in the X-ray spectrometer chamber is controlled within 35.0° ± 0.5°. The spectrometer's vertical divergence slit is 0.573°. Neither smoothing nor correction was applied to the raw data. For the energy calibration, the values of Deslattes *et al.*[14] were used as references for the diagram lines. The symmetric Si(220), Si(333), Si(440), Ge(220), Ge(333), and Ge(440) planes, and their reflections, were used in both crystals. The observed $K\alpha_{1,2}$ emission spectra of Cu are shown in Fig. 1. The stability of the instrument was evaluated in a recent study[15] for the Cu $K\alpha_{1,2}$ lines and a wide range of Kα, β diagram lines in 3d elements. Additionally, the $K\alpha_{1,2,3,4}$ spectra, recorded using the same spectrometer with a sealed Xe gas proportional counter, are shown in Fig. 2.

Table 1 Experimental conditions in spectral line measurements: (a) $K\alpha_{1,2}$ lines; (b) the $K\alpha_{1,2,3,4}$ lines. The tube operated at 40 kV and 60 mA. A Cu plate was used for all the measurements

Crystal	Step in 2θ (deg)	Integr. time (s)	Target	Times
(a)				
Si(220)	0.0005	4	Rh(SPC)	4
Si(333)	0.002	150	Rh(SPC)	10
Si(440)	0.0005	115	Rh(SPC)	3
Ge(220)	0.0005	0.5	Rh(SPC)	4
Ge(333)	0.001	50	W(FPC)	5
Ge(440)	0.0005	20	Rh(SPC)	3
(b)				
Si(220)	0.001	150	Rh(SPC)	3

The instrumental function of the double-crystal spectrometer can be very well described from Monte Carlo simulations as has been shown in ref. 11 and 16–18 and by simply computing the rocking curve of the Si crystals through dynamical diffraction theory.[17] From this instrumental function, one can obtain the natural linewidths as well as some other broadening mechanisms. In the present case, given the large natural widths of the diagram lines of neutral atoms when compared to the spectrometer instrumental function, we can use the simple broadening method described by Tochio *et al.*[10] without increasing the final uncertainty.

3 Theoretical procedures

3.1 Relativistic multiconfigurational calculations

The multiconfiguration Dirac–Fock (MCDF) method[19–21] and the multiconfiguration Dirac–Hartree–Slater (MCDHS) method[22] were used to calculate all the quantities needed to obtain the natural width, namely radiative and radiationless transition probabilities between levels. In this work, the radiative contributions were obtained using the General-purpose Relativistic Atomic Structure Program (GRASP) package,[19–21] and the non-radiative ones using the Flexible Atomic Code (FAC) developed by Gu.[22]

In the MCDF method, the effective relativistic Hamiltonian for an N-electron atom has the form:

$$\hat{H} = \sum_{i=1}^{N} \hat{h}_{\mathrm{D}}(i) + \sum_{j>i=1}^{N} V_{\mathrm{B}}(i,j), \quad (1)$$

where $\hat{h}_{\mathrm{D}}(i)$ is the one-electron Dirac Hamiltonian for the i-th electron. The term $V_{\mathrm{B}}(i,j)$ is a sum of the Coulomb interaction and the Breit operators, describing the interaction between the i-th and the j-th electrons.

The wave function for the N-electron system (characterized by the quantum numbers determining the value of the square of the total angular momentum J, projection of the angular momentum in the chosen direction M, and parity p) in the MCDF method is assumed in the form:

$$\Psi_s(JM^p) = \sum_m c_m(s)\Phi(\gamma_m JM^p), \quad (2)$$

where $\Phi(\gamma_m JM^p)$ represents N-electron configuration state functions (CSFs), $c_m(s)$ represents the configuration mixing coefficients for state s, and γ_m represents all information

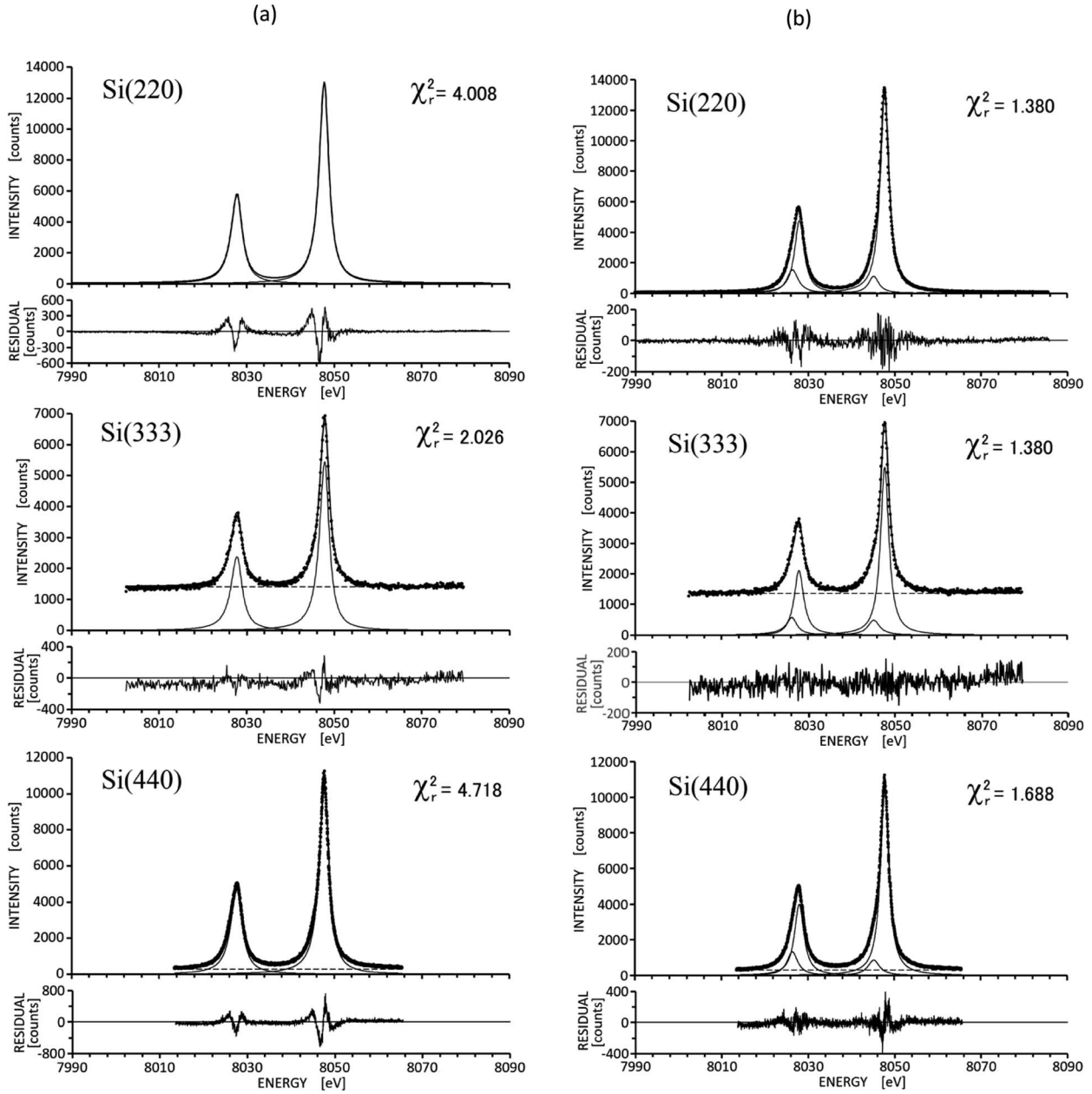

Fig. 1 A multiple peak fitting analysis with: (a) two asymmetric Cu K$\alpha_{1,2}$ lines measured using the spectroscopic crystals Si(220), Si(333) and Si(440); (b) four symmetric Cu K$\alpha_{1,2}$ lines measured using the spectroscopic crystals Si(220), Si(333) and Si(440).

required to uniquely define a certain CSF. The function $\Phi(\gamma_m JM^p)$ is an N-electron function given in the form of a Slater determinant or a combination of Slater determinants built from one-electron Dirac spinors. Moreover, in the calculations, it was necessary to include the Breit correction to the Coulomb repulsion operator and quantum electrodynamics corrections to energy, the so-called QED corrections, *i.e.*, self-energy and vacuum polarization. Using a finite-size nucleus model in the calculations was also crucial, including a two-parameter Fermi charge distribution. In general, the MCDHS method is similar to the MCDF method, but a simplified expression for the electronic exchange integrals has been used.[22]

3.2 Natural width of atomic levels

Due to the energy-time uncertainty principle ($\Delta E \Delta t \geq \hbar$), the lifetime of the excited state τ is connected with the natural width of the corresponding atomic level Γ by the relations

$$\Gamma = \frac{\hbar}{\tau} = \hbar\left(\sum_i X_i + \sum_j A_j + \sum_k C_k\right), \quad (3)$$

where X_i is the transition rate of the radiative process, A_j is the transition rate of the non-radiative Auger process, and C_k is the transition rate of the non-radiative Coster–Kronig (CK) process.

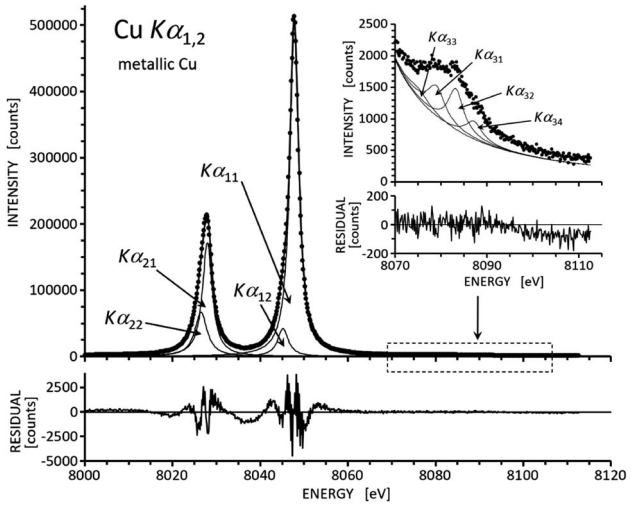

Fig. 2 Cu $K\alpha_{1,2,3,4}$ diagram lines and satellite lines are measured using the double-crystal X-ray spectrometer with a sealed Xe gas proportional counter. Eight symmetric Lorentz function fitting analyses were carried out for this element. The fitting results of one of the three measurements are shown in the figure.

The natural width of the atomic level of the i-th hole can be obtained in the form of a sum of the natural radiative width Γ_i^{rad} and the natural nonradiative width Γ_i^{nrad} of the i-hole state:

$$\Gamma_i = \Gamma_i^{\mathrm{rad}} + \Gamma_i^{\mathrm{nrad}} = \Gamma_{X_i} + \Gamma_{A_i} + \Gamma_{C_i}. \quad (4)$$

The natural widths of the $K\alpha_1$ and the $K\alpha_2$ X-ray radiative transitions can be expressed as follows

$$\Gamma_{K\alpha_1} = \Gamma_K + \Gamma_{L_3}, \quad (5)$$

$$\Gamma_{K\alpha_2} = \Gamma_K + \Gamma_{L_2}, \quad (6)$$

where Γ_K is the natural width of the initial atomic level with a hole in the K shell, and Γ_{L_2} and Γ_{L_3} are the natural widths of the final atomic levels with holes in the L_2 and L_3 subshells, respectively. The natural linewidths' data obtained through these procedures are shown in Tables 2–4.

4 Results and discussion

4.1 Experimentally estimated natural linewidths in Cu $K\alpha_{1,2}$ spectra

Cu $K\alpha_{1,2}$ spectra have been recorded more than three times each, using a high-resolution double-flat-crystal X-ray spectrometer. In the double crystal X-ray spectrometer, the natural line widths of the emission lines can be precisely extracted through several different procedures. The values of the averaged line energies, averaged FWHM, averaged corrected FWHM, and averaged relative intensity ratio for each line are obtained, using the procedure provided in Igor Pro (HULINKS Inc.),[9] as shown in Table 2.

To obtain the correct value for the natural linewidths of the Cu Kα lines, we performed a detailed study of these lines using Si and Ge crystals and several Bragg surfaces. The results are presented in Table 5. When higher-order crystal surfaces are used, the spectrometer adjustment is extremely difficult. Therefore, to obtain natural linewidths from the recorded spectra with this double-crystal X-ray spectrometer, the best procedure consists in using a low-order crystal plane and estimating the natural width by correcting for the instrumental function. We find Si crystals to be the best choice for the evaluation of the instrumental function in devices using spectroscopic crystals. The crystalline integrity of the Si crystals used in this work was confirmed by X-ray topography.

The best correction value for $K\alpha_{1,2}$ is obtained by using Si(220) planes, as seen in Fig. 3 and Table 5. Furthermore, from the same table, the area intensity of $K\alpha_{12}$ + $K\alpha_{22}$ satellite lines, resulting from the shake process,[5,6,8] relative to the total area, is ~15%, very close to the values in Melia *et al.*[26] and references therein. The widths of the Cu $K\alpha_1$ and $K\alpha_2$ lines obtained from these spectra are 2.260 eV for the $K\alpha_{11}$ line ($K\alpha_1$ line) and

Table 2 Natural radiative width of K, L_2, and L_3 levels

Contribution	Coulomb gauge (eV)	Babushkin gauge (eV)
$K^{-1} \rightarrow L_{2,3}{}^{-1}$	0.5834	0.6017
$K^{-1} \rightarrow M_{2,3}{}^{-1}$	0.0763	0.0795
$K^{-1} \rightarrow M_{4,5}{}^{-1}$	0.0001	0.0001
K level sum	0.6598	0.6813
$L_2{}^{-1} \rightarrow M_1{}^{-1}$	0.0003	0.0004
$L_2{}^{-1} \rightarrow M_{4,5}{}^{-1}$	0.0054	0.0061
L_2 level sum	0.0057	0.0065
$L_3{}^{-1} \rightarrow M_1{}^{-1}$	0.0003	0.0004
$L_3{}^{-1} \rightarrow M_{4,5}{}^{-1}$	0.0053	0.0060
L_3 level sum	0.0056	0.0064

Table 3 Natural nonradiative width of K, L_2, and L_3 levels

Contribution	Width (eV)
K − LL	0.6472
K − LM	0.1596
K − LN	0.0017
K − MM	0.0097
K − MN	0.0002
K level sum	0.8184
L_2 − L_3M	
L_2 − L_3N	0.0042
L_2 − MM	0.6170
L_2 − MN	0.0018
L_2 level sum	0.6230
L_3 − MM	0.6378
L_3 − MN	0.0016
L_3 level sum	0.6394

Table 4 Natural width of $K\alpha_1$ and $K\alpha_2$ lines

Line	Coulomb gauge (eV)	Babushkin gauge (eV)
$\Gamma_{K\alpha_1}$	2.1231	2.1454
$\Gamma_{K\alpha_2}$	2.1068	2.1292

2.530 eV for the $K\alpha_{21}$ line ($K\alpha_2$ line), respectively, as seen in Table 5. The width of the Cu $K\alpha_2$ line is likely to be enhanced by the contribution of the $L_2 - L_3M_{4,5}$ CK transition. The width of this CK transition will be within the energy range limited by the difference between ($K\alpha_2$ linewidth − $K\alpha_1$ linewidth), where it is assumed that the shake process is included in each spectrum

Table 5 Results from multiple peak analysis of Cu $K\alpha_{1,2}$ lines measured using various crystal planes. The analysis shows the results of asymmetry fitting of two peaks ($K\alpha_1$ and $K\alpha_2$) and symmetry fitting of four peaks ($K\alpha_{11}$, $K\alpha_{12}$, $K\alpha_{21}$ and $K\alpha_{22}$). Si*(220) is from Ito *et al.*[15] The averaged energy value, averaged FWHM, averaged asymmetry index (AI) or averaged corrected FWHM (CF), and averaged relative intensity of each spectrum are specified for each spectral crystal

	Lines	Energy	FWHM	AI	CF	Rel. int.	Area (%)
Si(220)	$K\alpha_1$	8047.780(42)	2.698(10)	1.145(9)		100	
	$K\alpha_2$	8027.823(40)	3.104(19)	1.158(15)		50.71(21)	
	$K\alpha_1 - K\alpha_2$	19.953(12)	0.406(21)				
	$K\alpha_{11}$	8047.780(42)	2.414(18)		2.264(18)	100	60.08
	$K\alpha_{12}$	8045.227(67)	2.87(14)			10.00(91)	6.01
	$K\alpha_{21}$	8028.034(60)	2.679(73)		2.534(73)	40.40(2.57)	24.27
	$K\alpha_{22}$	8026.45(11)	3.23(12)			16.04(2.90)	9.64
	$K\alpha_{11} - K\alpha_{21}$	19.746(31)			0.270(75)		
Si(333)	$K\alpha_1$	8047.842(69)	2.643(23)	1.228(19)		100	
	$K\alpha_2$	8027.754(66)	3.147(42)	1.186(35)		51.44(55)	
	$K\alpha_1 - K\alpha_2$	20.088(29)	0.504(48)				
	$K\alpha_{11}$	8047.798(68)	2.338(34)		2.298(34)	100	59.31
	$K\alpha_{12}$	8045.32(14)	3.11(33)			11.84(2.17)	7.02
	$K\alpha_{21}$	8027.933(75)	2.654(95)		2.617(95)	42.16(3.73)	25
	$K\alpha_{22}$	8026.34(14)	2.94(26)			14.63(4.18)	8.67
	$K\alpha_{11} - K\alpha_{21}$	19.865(44)			0.32(10)		
Si(440)	$K\alpha_1$	8047.762(46)	2.695(15)	1.198(9)		100	
	$K\alpha_2$	8027.731(42)	3.123(16)	1.171(10)		53.04(48)	
	$K\alpha_1 - K\alpha_2$	20.028(5)	0.428(22)				
	$K\alpha_{11}$	8047.747(68)	2.322(34)		2.296(27)	100	57.03
	$K\alpha_{12}$	8045.445(64)	3.70(13)			14.82(1.61)	8.45
	$K\alpha_{21}$	8027.909(39)	2.662(37)		2.638(37)	45.08(1.20)	25.71
	$K\alpha_{22}$	8026.310(35)	3.069(84)			15.46(1.40)	8.82
	$K\alpha_{11} - K\alpha_{21}$	19.838(44)			0.342(46)		
Ge(220)	$K\alpha_1$	8047.70(14)	3.242(16)	1.080(9)		100	
	$K\alpha_2$	8027.80(14)	3.645(23)	1.087(15)		50.86(25)	
	$K\alpha_1 - K\alpha_2$	19.902(20)	0.403(28)				
	$K\alpha_{11}$	8047.74(14)	2.982(28)		2.579(29)	100	60.72
	$K\alpha_{12}$	8045.14(14)	3.66(26)			8.98(1.54)	5.45
	$K\alpha_{21}$	8028.06(12)	3.229(80)		2.836(80)	41.08(2.91)	24.95
	$K\alpha_{22}$	8026.409(96)	3.78(15)			14.62(3.25)	8.88
	$K\alpha_{11} - K\alpha_{21}$	19.681(28)			0.257(85)		
Ge(333)	$K\alpha_1$	8047.828(70)	2.752(9)	1.227(9)		100	
	$K\alpha_2$	8027.783(77)	3.351(17)	1.221(25)		52.91(25)	
	$K\alpha_1 - K\alpha_2$	20.045(20)	0.599(19)				
	$K\alpha_{11}$	8047.789(71)	2.418(18)		2.362(18)	100	58.1
	$K\alpha_{12}$	8045.34(11)	3.40(15)			12.81(1.10)	7.44
	$K\alpha_{21}$	8027.954(82)	2.795(78)		2.743(78)	40.64(3.28)	23.61
	$K\alpha_{22}$	8026.51(15)	3.510(15)			18.66(3.29)	10.84
	$K\alpha_{11} - K\alpha_{21}$	19.835(28)			0.381(80)		
Ge(440)	$K\alpha_1$	8047.904(24)	2.778(12)	1.285(13)		100	
	$K\alpha_2$	8027.807(25)	3.470(25)	1.313(17)		55.58(21)	
	$K\alpha_1 - K\alpha_2$	20.097(2)	0.692(28)				
	$K\alpha_{11}$	8047.842(29)	2.389(18)		2.330(18)	100	55.14
	$K\alpha_{12}$	8045.467(88)	3.83(20)			15.40(1.23)	8.49
	$K\alpha_{21}$	8027.861(26)	2.64(13)		2.59(13)	35.16(4.43)	19.39
	$K\alpha_{22}$	8026.887(90)	4.71(15)			30.81(6.22)	16.99
	$K\alpha_{11} - K\alpha_{21}$	19.980(8)			0.26(13)		
Si(220)*	$K\alpha_1$	8047.773(75)	2.701(7)	1.142(6)		100	
	$K\alpha_2$	8027.813(81)	3.115(13)	1.158(9)		50.689(203)	
	$K\alpha_1 - K\alpha_2$	19.957(26)	0.414(15)				
	$K\alpha_{11}$	8047.773(76)	2.422(12)		2.273(12)	100	60.22
	$K\alpha_{12}$	8045.207(90)	2.871(84)			9.76(0.53)	5.88
	$K\alpha_{21}$	8028.038(82)	2.673(32)		2.527(32)	39.52(1.25)	23.8
	$K\alpha_{22}$	8026.476(92)	3.260(61)			16.77(1.29)	10.1
	$K\alpha_{11} - K\alpha_{21}$	19.736(24)			0.254(34)		

and ($K\alpha_{21}$ linewidth − $K\alpha_{11}$ linewidth), where the shake process is not included in these spectra, or between 0.41 eV and 0.27 eV, agreeing with the difference of Campbell and Papp recommended values[25] for the corresponding levels including the shake process, 0.43 eV, the experimental value of Yin *et al.*,[23] 0.44 eV, and the calculated value, 0.43 eV, for the CK transition reported by Ohno *et al.*[27]

The width of the CK transition was estimated to be in the range of 0.45 to 0.55 eV based on the excitation energy dependence of the Cu L_3/L_2 emission intensity ratio by Magnuson *et al.*[28] The value of Nyholm *et al.*,[29] 0.68 eV, is slightly larger. The calculated width of the $L_2 - L_3M_4$ CK transition by Yin *et al.*[23] is 0.287 eV. This value is well in agreement with our experimental value, not taking in account the [1s3d] shake processes.

The FWHM values of the $K\alpha_{11}$ line obtained with the Si(220) crystal planes and with the Ge(220) ones should, in principle, be the same, when the instrumental function is taken into account. However, we found the FWHM of the line obtained with the former crystal to be 0.3 eV less than the latter one. This difference suggests that the Ge crystal surface is probably not in good condition. However, when higher-order Ge lines are used, the half-widths of the $K\alpha_{11}$ and $K\alpha_{21}$ lines, corrected for the device function, are found to be closer to their natural widths.

To better visualize the above results, each FWHM (CF) obtained from the multiple peak fitting analysis, corrected by the instrument function, is plotted against the spectral crystal (2θ angle) in Fig. 3. The corrected values (CF) of the $K\alpha_1$ and $K\alpha_2$ linewidths obtained with the Ge(333) and Ge(440) planes are not as large as the values obtained with the Ge(220) ones. The use of higher-order Bragg planes removes the influence of the profile base, but the background is higher, which may be reflected in the natural width for the $K\alpha_2$ line. This seems to be particularly the case for Ge spectral crystals, although there may also be problems with crystal integrity.

From the theoretical point of view, as shown in Tables 2–4 and Fig. 3, the calculated natural widths of Cu $K\alpha_1$ and $K\alpha_2$ lines obtained in this work are 2.1231 eV and 2.1068 eV in the Coulomb gauge, and 2.1454 eV and 2.1292 eV in the Babushkin gauge, respectively.

Using the Γ_K width 1.49 eV from Campbell and Papp[25] and the Γ_{L_2} and Γ_{L_3} linewidths, obtained by Yin *et al.*[23] without the contribution of the $L_2 - L_3M_{4,5}$ CK transition, the $K\alpha_1$ and $K\alpha_2$ linewidths are 2.041 eV and 2.010 eV, respectively. The semi-empirical Cu linewidths from Krause and Oliver[24] are 2.11 eV for the $K\alpha_1$ line and 2.17 eV for the $K\alpha_2$ line, the Γ_K width being 1.554 eV. These values are also in good agreement with our calculations. It should be added that the calculated $K\alpha_2$ line broadening due to the $L_2 - L_3M_{4,5}$ CK transition for Cu is 0 eV, suggesting that in future more advanced theoretical and experimental studies are needed to explain this CK transition.

4.2 Cu $K\alpha_{3,4}$ satellites

The comparison between Ge and Si spectral crystals led us to conclude that the X-ray spectral measurement using reflections at the Si(220) Bragg planes is best with this spectrometer, due to the background effects of higher-order Bragg planes. The Cu $K\alpha_{1,2,3,4}$ lines measured using the Si(220) Bragg planes are shown in Fig. 2, with the conditions of this experiment presented in Table 1(b). The fitting analysis was performed for the eight peaks of the $K\alpha_{11,12,21,22}$ and $K\alpha_{31,32,33,34}$ diagram and satellite lines, using eight symmetric Lorentz functions. The results of the fitting analysis are shown in Table 6 together with the data reported by Mendenhall *et al.*[11] and Fritsch *et al.*[7] The results of the fitting analysis of the Lorentz functions of the four Cu $K\alpha_{1,2}$ lines by this study and Mendenhall *et al.* agree well, in terms of energy values and half-widths, including area intensity, as can be seen from Table 6. For the $K\alpha_{3,4}$ satellites, the results of Mendenhall *et al.* are almost twice as large as our results for the overall area intensity. In terms of energy values, Fritsch *et al.* reported the presence of the $K\alpha_{33}$ line near about 8070 eV, not seen in the present study and in the results of Mendenhall *et al.* In terms of intensity ratios, our observed $K\alpha_{32}/K\alpha_{31}$ intensity ratio is very close to the result of Mendenhall *et al.*, being only about a factor of 1.2 higher, and nearly twice as high as in Fritsch *et al.* We do not know the cause of this difference.

Furthermore, when the area intensities of the $K\alpha_{3,4}$ lines obtained by single crystal spectroscopy using Si(111)[30] and the intensity of the $K\alpha_{3,4}$ lines obtained through the analytical method of deconvolution are compared with the intensities of the $K\alpha_{3,4}$ lines obtained by high-resolution X-ray spectroscopy, the intensity of the $K\alpha_{3,4}$ lines obtained with Si(111) is the smallest.

4.3 Application to valence discrimination of the element in the compounds

From the numerical analysis considering the multiple peaks of Cu metal and Cr oxides,[15] we can obtain the energy value, FWHM, asymmetry index, and relative intensity ratio of atoms and compounds ((Kβ/Kα) ratio in the literature). In the future,

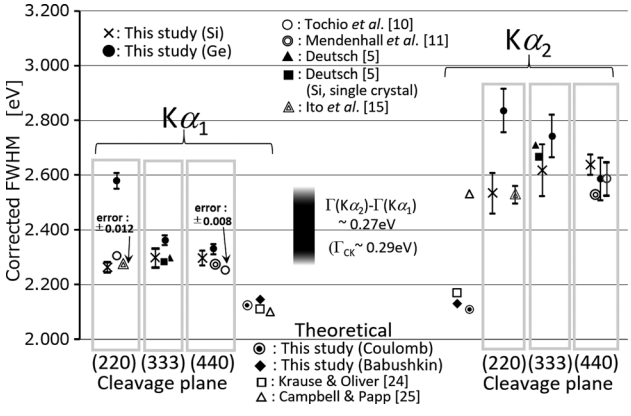

Fig. 3 The corrected FWHMs in the Cu $K\alpha_{1,2}$ diagram lines together with the data reported using a double-crystal or high-resolution X-ray spectrometer [Deutsch *et al.*,[5] Tochio *et al.*,[10] Mendenhall *et al.*,[11] and Ito *et al.*[15]]. The symmetric crystals, Si(220), Si(333), Si(440), Ge(220), Ge(333), and Ge(440) were used in this study, respectively. The Γ_{CK} value is taken from Yin *et al.*[23] Calculated values for both Coulomb and Babushkin gauges of the half-widths of the $K\alpha_{1,2}$ lines for Cu atoms are included with Krause and Oliver (semiempirical values),[24] and Campbell and Papp (recommended values).[25]

Table 6 Energy, Full Width at Half Maximum (FWHM), and Relative Intensity (R.I.) values in Cu $K\alpha_{1,2,3,4}$ spectra and satellite lines obtained in this study are presented, together with the data reported by Mendenhall *et al.*,[11] Fritsch *et al.*,[7] and Illig *et al.*[30] The asterisk in the FWHM in this study is corrected by the instrument function.[10] Note that the values from Fritsch *et al.* for R.I. are not normalized to the $K\alpha_{11}$ line intensity and cannot be directly compared with the values from the other authors

Lines	This study	Mendenhall	Fritsch	Illig
Energy				
$K\alpha_{11}$	8047.807(41)	8047.8254(3)		8047.947(18)
$K\alpha_{12}$	8045.221(28)	8045.2956(47)		8044.142(12)
$K\alpha_{21}$	8028.012(70)	8028.0503(27)		8028.272(17)
$K\alpha_{22}$	8026.567(74)	8026.5386(92)		8026.645(18)
$K\alpha_{11} - K\alpha_{21}$	19.8(5)	19.7751		
$K\alpha_{31}$	8079.12(34)	8078.627(58)	8078.0(3)	
$K\alpha_{32}$	8083.39(16)	8083.3528(38)	8082.7(1)	
$K\alpha_{33}$	8075.15(88)	8074.954(146)	8070.0(3)	
$K\alpha_{34}$	8087.50(34)	8088.109(57)	8087.5(2)	8076.623(25)
FWHM				
$K\alpha_{11}$	2.294(5)*	2.275(1)		2.484(2)
$K\alpha_{12}$	2.903(48)	2.915(9)		0.755(4)
$K\alpha_{21}$	2.531(25)*	2.529(5)		2.489(2)
$K\alpha_{22}$	3.428(37)	3.274(8)		3.089(2)
$K\alpha_{31}$	4.83(2.00)	5.51(14)	3.85(30)	
$K\alpha_{32}$	4.39(1.06)	5.51(14)	3.11(11)	
$K\alpha_{33}$	5.75(3.15)	3.22(21)	1.29(47)	
$K\alpha_{34}$	3.52(1.35)	3.22(21)	1.70(1.9)	3.844(3)
R.I.				
$K\alpha_{11}$	100	100		100
$K\alpha_{12}$	9.99(25)	12.123		1.4
$K\alpha_{21}$	37.36(89)	39.13		37.867
$K\alpha_{22}$	19.00(90)	19.284		14.683
$K\alpha_{31}$	0.20(13)	0.391	36.30(3.90)	
$K\alpha_{32}$	0.240(88)	0.465	67.7(4.0)	
$K\alpha_{33}$	0.075(90)	0.041	5.00(1.00)	
$K\alpha_{34}$	0.074(46)	0.087	1.40(62)	0.332

from the spectral measurement and analysis of Kα and Kβ lines by such high-resolution double crystal X-ray spectroscopy equipment, it is expected that various compounds including functional materials will be made into data based on the energy value, FWHM, asymmetry index, and intensity ratio of various compounds. Quantitative analysis of compounds with mixed valences can also be performed.[31]

5 Summary

Cu is a standard element for X-ray diffraction and X-ray spectroscopy, but there are many reports on the natural width of $K\alpha_{1,2}$ lines, and the values vary. Therefore, we measured the natural width of the $K\alpha_{1,2}$ line of Cu using two kinds of analyzing crystals, Si and Ge, using a high-resolution double-crystal X-ray spectrometer with an appropriate instrument function. By comparing the energy value, half width, asymmetry index, *etc.*, we found that the Si crystal is the most suitable for this spectrometer. The half widths obtained from this measurement were compared with the theoretically calculated values, 2.1231 and 2.1454 eV for the $K\alpha_1$ line, and 2.1068 eV and 2.1292 eV for the $K\alpha_2$ line, in the Coulomb and Babushkin gauges, respectively. The calculations show that the contribution of the $L_2 - L_3M_{4,5}$ CK transition is negligible and cannot explain the difference in the $K\alpha_1$ and $K\alpha_2$ experimental linewidth values. Therefore, it is necessary to perform more advanced theoretical calculations and sophisticated experiments on this CK transition. We also measured the profile of $K\alpha_{3,4}$ satellites, due to the [1s2p] shake process, using the spectrometer and the Si(220) planes, this crystal having the best S/B ratio among the three analysing crystals. The half-width and intensity ratio were determined.

Author contributions

Conceptualization: Y. Ito, M. Polasik, and F. Parente; data curation: M. Yamashita and S. Fukushima; formal analysis: Y. Ito, T. Tochio, S. Fukushima, Ł. Syrocki, K. Słabkowska, M. Polasik, J. P. Marques, and F. Parente; funding acquisition: Y. Ito, F. Parente, J. P. Marques, and M. Polasik; investigation: Y. Ito, M. Yamashita, S. Fukushima, and T. Tochio; methodology: Y. Ito, Ł. Syrocki, K. Słabkowska, and M. Polasik; software: S. Fukushima; supervision: Y. Ito; validation: Y. Ito, M. Polasik, J. P. Marques, and F. Parente; visualization: Ł. Syrocki, J. P. Marques, and F. Parente; writing – original draft: Y. Ito, M. Polasik, and F. Parente; writing – review & editing: Y. Ito, Ł. Syrocki, K. Słabkowska, J. P. Marques, and F. Parente.

Conflicts of interest

There are no conflicts to declare.

Acknowledgements

Y. Ito acknowledges the financial support for the measurements of a part of the data by the REXDAB Collaboration that was initiated within the International Fundamental Parameter Initiative. This research was supported in part by FCT (Portugal) under research center grants UID/FIS/04559/2020 (LIBPhys) and UIDP/50007/2020 (LIP). This work was also supported by the National Science Centre, Poland, under grant number 2021/05/X/ST2/01664.

Notes and references

1 M. Druyvesteyn, *Z. Phys.*, 1928, **43**, 707.
2 S. Doniach and M. Sunjic, *J. Phys.*, 1970, **C3**, 285.
3 K. Tsutsumi and H. Nakamori, in *X-Ray Spectra and Electronic Structure of Matter*, Fotodruck Frank OHG, Munich, 1973.
4 J. Finster, G. Leonhardt and A. Meisel, *J. Phys., Colloq.*, 1971, **32**, C4–218.
5 M. Deutsch, G. Hölzer, J. Härtwig, J. Wolf, M. Fritsch and E. Förster, *Phys. Rev. A: At., Mol., Opt. Phys.*, 1995, **51**, 283–296.
6 M. Deutsch, O. Gang, G. Hölzer, J. Härtwig, J. Wolf, M. Fritsch and E. Förster, *Phys. Rev. A: At., Mol., Opt. Phys.*, 1995, **52**, 3661.

7 M. Fritsch, C. C. Kao, K. Hamalainen, O. Gang, E. Förster and M. Deutsch, *Phys. Rev. A: At., Mol., Opt. Phys.*, 1998, **57**, 1686.
8 Y. Ito, T. Tochio, H. Ohashi, M. Yamashita, S. Fukushima, M. Polasik, K. Słabkowska, Ł. Syrocki, E. Szymańska, J. Rzadkiewicz, P. Indelicato, J. P. Marques, M. C. Martins, J. P. Santos and F. Parente, *Phys. Rev. A: At., Mol., Opt. Phys.*, 2016, **94**, 042506.
9 Y. Ito, T. Tochio, M. Yamashita, S. Fukushima, A. M. Vlaicu, J. P. Marques, J. M. Sampaio, M. Guerra, J. P. Santos, Ł. Syrocki, K. Słabkowska, E. Weder, M. Polasik, J. Rzadkiewicz, P. Indelicato, Y. Ménesguen, M.-C. Lépy and F. Parente, *Phys. Rev. A: At., Mol., Opt. Phys.*, 2020, **102**, 052820.
10 T. Tochio, Y. Ito and K. Omote, *Phys. Rev. A: At., Mol., Opt. Phys.*, 2002, **65**, 042502.
11 M. H. Mendenhall, A. Henins, L. T. Hudson, C. I. Szabo, D. Windover and J. P. Cline, *J. Phys. B: At., Mol. Opt. Phys.*, 2017, **50**, 115004.
12 Y. Ito, T. Tochio, M. Yamashita, S. Fukushima, A. M. Vlaicu, Ł. Syrocki, K. Słabkowska, E. Weder, M. Polasik, K. Sawicka, P. Indelicato, J. P. Marques, J. M. Sampaio, M. Guerra, J. P. Santos and F. Parente, *Phys. Rev. A: At., Mol., Opt. Phys.*, 2018, **97**, 052505.
13 Y. Ménesguen, M. C. Lépy, Y. Ito, M. Yamashita, S. Fukushima, T. Tochio, M. Polasik, K. Słabkowska, Ł. Syrocki, P. Indelicato, J. P. Gomilsek, J. P. Marques, J. M. Sampaio, J. Machado, P. Amaro, M. Guerra, J. P. Santos and F. Parente, *Radiat. Phys. Chem.*, 2022, **194**, 110048.
14 R. D. Deslattes, E. G. Kessler, P. Indelicato, L. de Billy, E. Lindroth and J. Anton, *Rev. Mod. Phys.*, 2003, **75**, 35–99.
15 Y. Ito, M. Yamashita, T. Tochio, M. Yamashita, S. Fukushima, T. Shoji, K. Słabkowska, Ł. Syrocki, M. Polasik, J. P. Gomilsek, J. P. Marques, J. M. Sampaio, M. Guerra, J. Machado, J. P. Santos, A. Hamidani, A. Kalhoul, P. Indelicato and F. Parente, *Int. J. Mol. Sci.*, 2023, **24**, 5570.
16 J. Machado, C. I. Szabo, J. P. Santos, P. Amaro, M. Guerra, A. Gumberidze, G. Bian, J. M. Isac and P. Indelicato, *Phys. Rev. A: At., Mol., Opt. Phys.*, 2018, **97**, 032517.
17 J. Machado, G. Bian, N. Paul, M. Trassinelli, P. Amaro, M. Guerra, C. I. Szabo, A. Gumberidze, J. M. Isac, J. P. Santos, J. P. Desclaux and P. Indelicato, *J. Phys. B: At., Mol. Opt. Phys.*, 2019, **52**, 215004.
18 J. Machado, G. Bian, N. Paul, M. Trassinelli, P. Amaro, M. Guerra, C. I. Szabo, A. Gumberidze, J. M. Isac, J. P. Santos, J. P. Desclaux and P. Indelicato, *Phys. Rev. A: At., Mol., Opt. Phys.*, 2020, **101**, 062505.
19 K. Dyall, I. Grant, C. Johnson, F. Parpia and E. Plummer, *Comput. Phys. Commun.*, 1989, **55**, 425–456.
20 F. Parpia, C. Fischer and I. Grant, *Comput. Phys. Commun.*, 1996, **94**, 249–271.
21 P. Jönsson, X. He, C. Froese Fischer and I. Grant, *Comput. Phys. Commun.*, 2007, **177**, 597–622.
22 M. F. Gu, *Can. J. Phys.*, 2008, **86**, 675–689.
23 L. I. Yin, I. Adler, M. H. Chen and B. Crasemann, *Phys. Rev. A: At., Mol., Opt. Phys.*, 1973, **7**, 897.
24 M. Krause and J. Oliver, *J. Phys. Chem. Ref. Data*, 1979, **8**, 329.
25 J. Campbell and T. Papp, *At. Data Nucl. Data Tables*, 2001, **77**, 1.
26 H. A. Melia, C. T. Chantler, L. F. Smale and A. J. Illig, *Acta Crystallogr., Sect. A: Found. Adv.*, 2019, **75**, 527.
27 M. Ohno, J. M. Mariot and C. F. Hague, *J. Electron Spectrosc. Relat. Phenom.*, 1985, **36**, 17.
28 M. Magnuson, N. Wassdahl and J. Nordgren, *J. Phys. B: At., Mol. Opt. Phys.*, 1997, **56**, 12238.
29 R. Nyholm, N. Martensson, A. Lebuglet and U. Axelsson, *J. Phys. F: Met. Phys.*, 1981, **11**, 1727.
30 A. J. Illig, C. T. Chantler and A. T. Payne, *J. Phys. B: At., Mol. Opt. Phys.*, 2013, **46**, 235001.
31 T. Tochio, S. Sakakura, H. Oohashi, H. Mizota, Y. Zou, Y. Ito, S. Fukushima, S. Tanuma, T. Shoji, H. Fujimura and M. Yamashita, *Anal. Sci.*, 2010, **26**, 277.